Exploring the hydrodynamics of Mixed Wave Energy farms

Raghavan, Vaibhav; Metrikine, Andrei; Lavidas, George

DOI
10.36688/ewtec-2025-699

Publication date
2025

Document Version
Final published version

Published in
Proceedings of the European Wave and Tidal Energy Conference

Exploring the hydrodynamics of Mixed Wave Energy farms

V. Raghavan, A.V. Metrikine, and G. Lavidas

Abstract—**In order to reduce the Levelized Cost Of Energy (LCOE) of Wave Energy Converters (WECs) and make them competitive with conventional energy sources, they would need to be deployed in large numbers as farms similar to Offshore Wind. Given their significant capacity, Offshore wind turbines are often placed at large distances apart, to reduce destructive wake effects, while maintaining a high energy density per unit area. However, WECs within a farm, are much smaller with much lower capacities and stronger inter device interactions due to the presence of a highly dense fluid. Therefore, larger number of WECs can be deployed in closer proximity to produce comparable energy density per unit area. As we move towards hybrid systems with floating solar, wind and wave energy amongst others, efficiency in deployment within an area becomes key. Conventional wave farm concepts that have been extensively studied such as 1) wave farms of different types of WECs (Point Absorber or PA, Attenuator, Flap etc) also referred to as homogeneous farms (same device in multiple numbers) and 2) wave farms with different sizes and drafts of one type of WEC also referred to as heterogeneous farms. To date, studies have focused on multiple devices with similar geometries interacting through the same degrees of freedom. With this research, the authors explore mixed wave energy farms, which are wave farms utilizing different types of wave energy converters in the same farm. With the focus on the hydrodynamics and power produced by wave energy converters, this research provides for the first time insights into the interaction of devices, with varying geometries and degrees of freedom, thus entering an entirely new domain of wave farm research. As a case study, the authors look into a mixed farm of PAs and flaps and compare them with mono-farms of the same devices.**

Index Terms—**Mixed farms, BIEM, HAMS-MREL, m-factor**

I. Introduction

In order to reach the high targets of 1 GW by 2030 and 40 GW by 2050 [1], WECs need to be deployed in large numbers. Many WEC devices including the Corpower C4 point absorber device [2] and AW WaveRoller oscillating surge device [3], alongside others, are on their way to commercial deployment in wave energy farms. The HiWave-5 project from Corpower is set to test a 4 WEC farm (One C4 and three C5 WECs) off the coast of Agucadoura, Northern Portugal [4]. The Ondas de Peniche (ONDEP) project aims to deploy a 2 MW wave energy farm featuring four Waveroller WECs off the coast of Peniche, Portugal in the next five years [5]. Therefore, research focused on the study of such devices, particularly in wave farms has become highly relevant. This requires computationally efficient tools that can capture wave-structure hydrodynamic interactions considering multiple bodies.

Mono-farms refer to farms/arrays of the same device with the same geometry, size and structural properties deployed in multiple numbers (>1). These are currently the most commonly studied farms, whether it is academic research or commercial deployment (Some examples were given earlier). There are numerous experimental and numerical studies focused on the hydrodynamics, power production and optimization of mono-farms with PAs ([6]–[24]), flaps ([25], [26]), attenuators ([10], [27]) and Oscillating Water Columns (OWCs) [28]. The employed hydrodynamic models for the WECs vary from low fidelity frequency domain models with Boundary Integral Equation Method (BIEM) to high fidelity Computational Fluid Dynamics (CFD) models with Smooth Particle Hydrodynamics (SPH).

Going a step further, being able to derive more power from the same number of devices over a range of periods will increase the energy density per unit area obtained from WECs, thus making wave energy more efficient. Therefore, numerical investigations have also been extended to 'heterogeneous' and 'hybrid' wave farms.

Heterogeneous wave farms employ the same type of wave energy converter while changing the size, or draft or a combination of both. Goteman [29] studied farms with cylindrical PAs, with varying diameters with and without moonpools. The analytical method based on multiple scattering method utilizing the hydrodynamic coefficients from WAMIT was used for assessing the hydrodynamics. When studying farms of four devices, it was found that considering two cylinders with moonpool and two without (varying the inner/outer radius) gave 2.9% more power than mono farms with one type of device. Furthermore, farms of 12 devices were investigated with different diameters with 1000 different layouts. The difference in power absorption between the best and worst layout was found to be 23 %. Ermakov et.al. [30] investigated the optimization of heterogeneous farms with using a control co-design approach, utilizing the enforcement of displacement constraints in the frequency domain. The methodology was utilized for 3 to 5 cylindrical point absorber devices considering multi-directional wind and ocean waves. Results showed that the improvements in power produced by the farm as compared to these devices in isolation could be up to 37% to 72.2%

V. R., A. M. and G. L. are part of the Offshore Engineering Section of the Delft University of Technology (TU Delft), Stevinweg 1, 2628 CN Delft, The Netherlands (e-mail: v.raghavan@tudelft.nl, a.metrikine@tudelft.nl, g.lavidas@tudelft.nl).

Digital Object Identifier:
https://doi.org/10.36688/ewtec-2025-699

from 3 to 5 WECs. Abdulkadir et.al. [31] performed a frequency domain based optimization of heterogeneous farms (varying diameter) of cylindrical devices using a time domain model with Power-Constrained Bang-Singular-Bang (PCBSB) control. Detailed simulation of homogeneous and heterogeneous farms showed an average performance improvement of 6.6%, 20.02% and 9.71% for 3,5 and 7 devices for a representative wave period of 6 s and wave height of 0.82 m.

'Hybrid' farms were investigated in the work of Zheng et.al. [28], which analyses the performance of farms comprising of cylindrical PAs and cylindrical OWCs with varying diameters/drafts. Hybrid farms of 4 devices with 2 PA and 2 OWCs were investigated and evaluated using the H-factor, that shows if the hybrid farm is more constructive or destructive compared to the mono-farm by taking the ratio of the power produced by a hybrid farm to a mono-farm. For some wave periods, H-factor as high as 1.6 were obtained for the hybrid farms. The H-factor is also used later in the current study.

The current study introduces 'Mixed' farms, a concept that is completely new, which are wave farms utilizing different types of wave energy converters operating in different degrees of freedom in the same farm/array. Wolgamot et.al. [9] briefly investigated an optimized farm of three devices (ellipsoid, elliptical cylinder and hemisphere) operating in heave, surge and sway respectively under regular waves. Investigation was performed into the influence of directionality on the power produced by the farm, however the gain in power with respect to the mono farms was not investigated. This study provides more insight into the performance of mixed farms comparing them with mono farms.

II. Hydrodynamics of single wave energy devices

A. Device Description

For this study, two wave energy converters are utilised. The first device is the PA, which is one of the most common wave energy converter types. The geometry of this device is inspired from the state-of-the-art Corpower C4 WEC. The second device is the bottom-fixed flap, inspired by the state-of-the-art Waveroller WEC.

The geometry and mass properties of the PAs are shown in Table I. These have been taken from a previous study [32]. The draft of 6 m was assumed by the authors for this study and the natural frequency was calculated based on the aforementioned properties. The geometry and mass properties of the flap device are shown in Table II, and were taken from [33]. The draft of 9 m was considered based on for this study and the natural frequency was calculated based on the aforementioned properties.

B. Equations of motion and BEM

A weakly non-linear frequency domain model is developed, only considering heave motion for point absorber and pitch motion for the flap. These are used for estimating the motion of the respective device per frequency, considering viscous losses.

For both the flap and PA, a linear passive control PTO (Power Take-Off) is considered. The PTO damping coefficient is optimized based on the work of Hals et.al. [34] considering viscous losses without constraints, which will be explained later. The motion of the PA for the i^{th} frequency ω_i is estimated with the following expression:

$$[-\omega_i^2(m_d + m_a(\omega_i)) + i\omega_i\Big(b_a(\omega_i) + b_{PTO}(\omega_i) + b_v\Big) + c_h]\, s(\omega_i) = f_e(\omega_i) \tag{1}$$

where the inertia term is the combinations of are the mass m_d and the added mass heave hydrodynamic coefficient m_a of the PA. Then, b_a is the radiation damping heave hydrodynamic coefficient, b_{PTO} is the PTO coefficient for the device, b_v is the linearized viscous damping coefficient. Finally, c_h is the hydrostatic stiffness coefficient in heave, f_e is the heave exciting force, and s is the displacement amplitude of the device also referred to as the body excursion. Similarly, the motion of the flap for the i^{th} frequency ω_i is estimated with the following expression:

$$[-\omega_i^2(I_d + I_a(\omega_i)) + i\omega_i\Big(B_a(\omega_i) + B_{PTO}(\omega_i) + B_v\Big) + C_h]\theta(\omega_i) = M_e(\omega_i) \tag{2}$$

where the inertia term is the combinations of are the moment of inertia I_d and the added mass pitch hydrodynamic coefficient I_a of the flap. Then, B_a is the radiation damping pitch hydrodynamic coefficient, B_{PTO} is the PTO coefficient for the device, B_v is the linearized viscous damping coefficient in pitch. Finally, C_h is the hydrostatic stiffness coefficient in pitch, M_e is

TABLE I
PROPERTIES OF THE PA DEVICE

Property	Value	Unit
Diameter	9	m
Height	18	m
Installation depth (minimum)	40	m
Weight	70	T
Draft	6	m
Undamped Natural period (heave)	3	s

TABLE II
PROPERTIES OF THE FLAP DEVICE

Property	Value	Unit
Width	17.7	m
Height	10.6	m
Peak thickness	3.5	m
Moment of Inertia	8.8e6	kgm^2
Draft	9	m
Undamped Natural period (pitch)	17.2	s

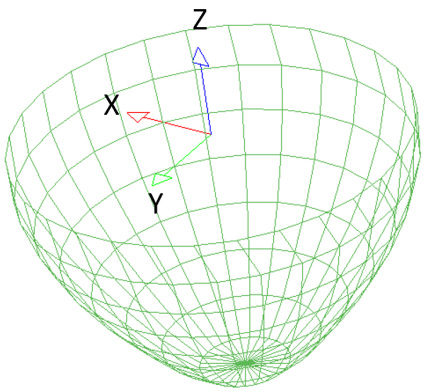

Fig. 1. Mesh of Point absorber modelled using HAMS-MREL

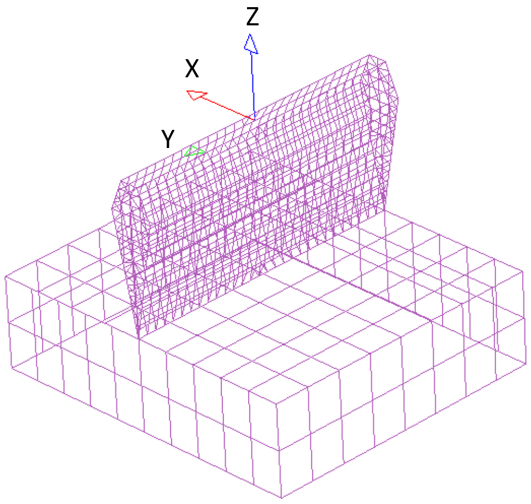

Fig. 2. Mesh of flap modelled using HAMS-MREL

the pitch moment exciting force, and θ is the rotation amplitude of the device.

When the amplitude of the incident wave is 1 m, then s or θ represents the RAO (Response amplitude Operator) in heave or pitch motion for the corresponding device. The viscous drag are not very important for the PA, however for the flap these can be quite important, even as small wave heights. This has been demonstrated in Da Silva et al. [35]. For completeness, it has been considered for both the PA and flap.

The frequency dependent hydrodynamic coefficients and exciting forces are obtained from the frequency domain Boundary Element Method (BEM) solver HAMS-MREL [36]. The PA mesh employed for running the simulations in HAMS-MREL is shown in Fig. 1 and for the flap mesh in Fig. 2. For the flap, an additional mesh for the concrete foundation was incorporated and its dimensions are based on [33]. The number of panels to be considered were based on a convergence study. To determine the hydrodynamic coefficients and excitation forces for the flap, the generalized modes approach, based on our previous work [37], was utilized.

C. PTO control and viscous effects

The optimized damping coefficient for the PA for any given frequency is given by

$$b_{PTO}(\omega_i) = (R(\omega_i)^2 + X(\omega_i)^2)^{1/2} \tag{3}$$

where

$$R(\omega_i) = b_a(\omega_i) + b_v \tag{4}$$

and

$$X(\omega_i) = i\omega_i[m_d + m_a(\omega_i)] + (c_h/i\omega_i) \tag{5}$$

When considering the regular wave condition, the viscous damping is computed using the expression from Lorentz linearization [38]. This is given as:

$$b_v = \frac{4}{3\pi} C_D \rho A_D \tag{6}$$

Here C_D is the drag coefficient in heave and A_D is the projected area in heave. Similar procedure is followed for the flap.

When considering shallow water depths, the orbital motion of the fluid is elliptical in nature. Moreover, the horizontal fluid particle velocity remains significant throughout the entire depth, in contrast to deep water conditions where velocities decrease rapidly with depth. Consequently, when calculating viscous forces, particularly for the flap, it may be important to account for the depth-dependent relative velocity.

In the study by Da Silva et al. [35], a statistical linearization of Morison's equation was performed for both a PA (in intermediate to deep water) and a flap (in shallow water), considering irregular sea states. Two cases were analyzed: one where only the structural velocity was used to calculate the viscous force, and another where the relative velocity (the difference between the structural and fluid velocities at various depths) was considered. It was observed that, for significant wave heights ranging from 1 to 3 meters and peak periods between 5 and 12 seconds (consistent with the present analysis), the average difference in absorbed power between the two approaches for the flap was approximately 15%, with the structural velocity only approach leading to an underestimation. Given this underestimation, using only the depth-dependent structural velocity (which is currently utilized) yields a more conservative estimate of the absorbed power compared to using the relative depth-dependent velocity.

When considering irregular waves, an iterative procedure utilizing spectral domain method ([39]–[41]) is adopted to compute the viscous damping coefficient and thus the response, which is described in detail in our work [42] (in press). The mean squared error for the iterative process is 1e-6. This approach is considered since it has shown to be capable of better capturing the viscous effects when considering irregular sea states [43]. The procedure above for obtaining the optimized PTO coefficient for the PA can be similarly utilized for the flap.

When considering the direction of the incident wave, for the PA, being axisymmetric, this direction does not matter. However, for the flap, direction perpendicular

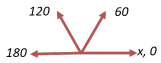

Fig. 3. Incident wave directions

to the width was chosen, since this would give the maximum power from the flap.

D. Power estimation

With regular waves, the power for a given frequency ω_i for the can be obtained as

$$P_{p,i} = \frac{1}{2} b_{PTO} \omega_i^2 |s_i|^2 \tag{7}$$

for the PA and as

$$P_{f,i} = \frac{1}{2} B_{PTO} \omega_i^2 |\theta_i|^2 \tag{8}$$

for the flap.

With irregular waves, for either PA or flap, the power can be computed as:

$$P_{irr} = \int_0^\infty 2P(\omega)S(\omega)d\omega \tag{9}$$

where $P(\omega)$ is the power spectra over all considered frequencies with power for the i^{th} frequency calculated using Eqn. 7 or Eqn. 8 depending on the device. $S(\omega)$ is the spectra for the considered sea state based on the Goda formulation [44] with the α obtained from [42].

III. Wave farm Analysis

A. Wave farm description

Wave farms of 10 devices are considered - two mono and one mixed. The two mono-farms are that of the PA and flap respectively. The spacing between the devices in the PA farm was taken as $L_p = 6D$, where D is the diameter of the PA. The spacing between the devices in the flap farm was taken as $L_f = 6W$, where W is the width of the flap. The mixed farm consists of five PAs and five flaps. For the mixed farm, the averaged spacing of $L_m = (L_p + L_f)/2$ is considered. The spacing is chosen to keep a relatively compact WEC array.

Two different configurations are considered - rectangular and staggered. Four incident wave directions are considered - 0, 60, 120 and 180 degrees with respect to the positive x axis (Long crested waves). These are shown in Fig. 3. For the irregular wave cases, this can be regarded as the dominant direction. This provides a total of 24 cases, which are summarized in Table III.

The configurations are shown in Figure 6-9.

B. Wave farm hydrodynamics

The weakly non-linear frequency domain model is developed for single devices (Eq. 1 and 2) is extended for farms. The equation of motion for the i^{th} for the farm (mono or mixed) can be obtained as:

$$[-\omega_i^2(\mathbf{M_d} + \mathbf{M_a}(\omega_i)) + i\omega_i(\mathbf{B_a}(\omega_i) + \mathbf{B_{PTO}}(\omega_i) + \mathbf{B_v}) + \mathbf{C_h}]\mathbf{S}(\omega_i) = \mathbf{F_e}(\omega_i) \tag{10}$$

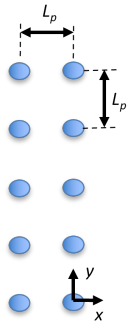

Fig. 4. PA farm rectangular configuration (not to scale)

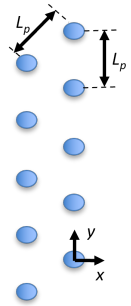

Fig. 5. PA farm staggered configuration (not to scale)

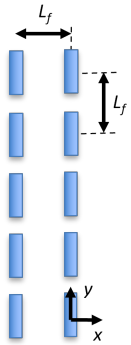

Fig. 6. Flap farm rectangular configuration (not to scale)

Fig. 7. Flap farm staggered configuration (not to scale)

TABLE III
CASES CONSIDERED FOR WAVE FARM ANALYSIS

Case name	Number of WECs	WEC type	Configuration	Direction (deg)
WECA-PA-STAG-0	10	PA	Staggered	0
WECA-PA-STAG-60	10	PA	Staggered	60
WECA-PA-STAG-120	10	PA	Staggered	120
WECA-PA-STAG-180	10	PA	Staggered	180
WECA-PA-RECT-0	10	PA	Rectangular	0
WECA-PA-RECT-60	10	PA	Rectangular	60
WECA-PA-RECT-120	10	PA	Rectangular	120
WECA-PA-RECT-180	10	PA	Rectangular	180
WECA-FL-STAG-0	10	Flap	Staggered	0
WECA-FL-STAG-60	10	Flap	Staggered	60
WECA-FL-STAG-120	10	Flap	Staggered	120
WECA-FL-STAG-180	10	Flap	Staggered	180
WECA-FL-RECT-0	10	Flap	Rectangular	0
WECA-FL-RECT-60	10	Flap	Rectangular	60
WECA-FL-RECT-120	10	Flap	Rectangular	120
WECA-FL-RECT-180	10	Flap	Rectangular	180
WECA-MIX-STAG-0	10 (5+5)	PA+Flap	Staggered	0
WECA-MIX-STAG-60	10 (5+5)	PA+Flap	Staggered	60
WECA-MIX-STAG-120	10 (5+5)	PA+Flap	Staggered	120
WECA-MIX-STAG-180	10 (5+5)	PA+Flap	Staggered	180
WECA-MIX-RECT-0	10 (5+5)	PA+Flap	Rectangular	0
WECA-MIX-RECT-60	10 (5+5)	PA+Flap	Rectangular	60
WECA-MIX-RECT-120	10 (5+5)	PA+Flap	Rectangular	120
WECA-MIX-RECT-180	10 (5+5)	PA+Flap	Rectangular	180

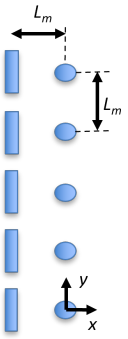

Fig. 8. Mixed farm rectangular configuration (not to scale)

Fig. 9. Mixed farm staggered configuration (not to scale)

where the inertia term is the combinations of are the diagonal mass matrix $\mathbf{M_d}$ and the fully populated added mass coefficient matrix $\mathbf{M_a}$. Then, $\mathbf{B_a}$ is the fully populated radiation damping coefficient matrix, $\mathbf{B_{PTO}}$ is the fully populated optimized PTO damping coefficient matrix, $\mathbf{B_v}$ is the diagonal linearized viscous damping coefficient matrix. Finally, $\mathbf{C_h}$ is the hydrostatic stiffness coefficient matrix, $\mathbf{F_e}$ is the excitation force column vector, and $\mathbf{S}$ is the response column vector. When the amplitude of the incident wave is 1 m, then S represents the RAO column vector.

In order to determine the optimized PTO damping coefficient matrix, the procedure in Section II-C is adapted for farms, and given as:

$$\mathbf{B}_{\mathrm{PTO}}(\omega_i) = \left((\mathbf{B_a}(\omega_i) + \mathbf{B_v})^2 + \left(\omega_i (\mathbf{M_d} + \mathbf{M_a}(\omega_i) - \frac{\mathbf{C_h}}{\omega_i} \right)^2 \right)^{\frac{1}{2}} \tag{11}$$

based on [45], [46]. When considering the regular wave condition, the viscous damping matrix is a diagonal matrix with the coefficient calculated based from Eqn. 6. When considering the irregular sea states, the procedure for single devices has been similarly extended for farms based on [42].

With regular waves, the power for a given frequency ω_i for farm the can be obtained as in Eqn 12:

$$P_{farm}(\omega_i) = \frac{1}{2}\omega_i^2 \widetilde{\mathbf{S}}^*(\omega_i)\mathbf{B_{PTO}}(\omega_i)\mathbf{S}(\omega_i) \tag{12}$$

When considering irregular waves, Eqn. 9 can be utilized as done for the single devices. The '~' and '*' is used to denote the complex conjugate.

IV. METRICS TO COMPARE WEC FARMS

For comparing the mono and mixed farms, both in regular and irregular waves, we use three metrics:

- q-factor - The q-factor is defined as the ratio of the power absorbed by the farm to that of the devices in isolation. This factor tells us if the given farm configuration is destructive (<1) or constructive (>1), considering the hydrodynamic interactions between WECs. This is given as:

$$q = \frac{P_{farm}}{m \cdot P_p + n \cdot P_f} \tag{13}$$

where m is the number of PA devices, n is the number of flap devices in the farm. P_p and P_f is the power absorbed by a PA and flap respectively, when they are in isolation. P_{farm} can be the mono or mixed farm.

- H-factor - This is referred to as the Hybrid factor, and was introduced by Zheng et.al. [28]. This tells us if the mixed farm performs equivalent or better than the mono-farms. This is given as:

$$H = \frac{P_{mixed}}{m \cdot q_p \cdot P_p + n \cdot q_f \cdot P_f} \tag{14}$$

This factor directly compares if the mixed farm is more constructive (H >1) or destructive (H <1) with respect to the mono-farms considering farm effects for both. Here m and n are the number of PAs and flaps in the mixed farm respectively.

- $M-$factor - Due to the differences in the dimensions of the WECs considered, it is also interesting to assess power absorbed per unit width of the device for devices in the mixed and mono-farms, and compare them. This can be expressed in terms of the capture width ratio as:

$$M = \frac{\eta_{mixed}}{(\frac{m}{m+n} \cdot \eta_p + \frac{n}{m+n} \cdot \eta_f)} \tag{15}$$

where, η_p and η_f are the capture width ratios of the PA and flap mono-farms respectively. The various capture width ratios are given as:

$$\eta_{mixed} = \frac{P_{mixed}}{(m \cdot D + n \cdot W) \cdot P_{inc}} \tag{16}$$

$$\eta_p = \frac{q_p \cdot P_p}{D \cdot P_{inc}} \tag{17}$$

$$\eta_f = \frac{q_f \cdot P_f}{W \cdot P_{inc}} \tag{18}$$

P_{inc} is the incident wave power expressed in kW/m. This factor normalizes the differences in the power produced from the devices due to differences in their dimensions, thus including the effect of the hydrodynamic interactions between the devices as well as the dimensions of the devices themselves. This factor will be referred to as the $M-$factor or the Mixed factor.

A. Wave data

For the analysis considering irregular waves, a location off the Dutch coast was utilized ((latitude: 53 ° 36′, longitude: 6 ° 18′) [47]. The scatter diagram (shown in Fig. 10) is only used as a reference for which sea states were considered in the calculation, and not for the power calculations themselves. About 32% of the occurrences are with H_s= 1 m, across T_p from 3 s to 12 s. These are the sea states considered for the analysis.

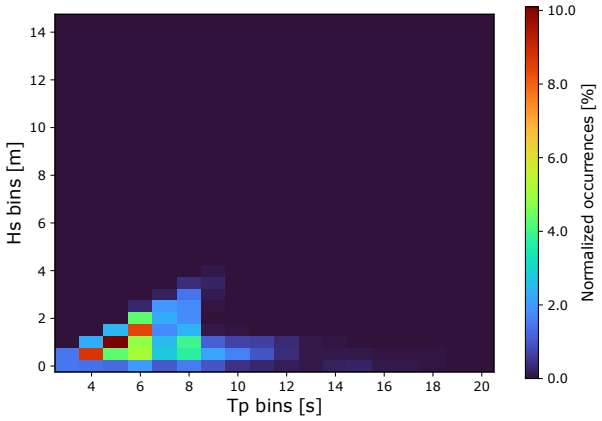

Fig. 10. Scatter diagram off the dutch coast(latitude: 53 ° 36′, longitude: 6 ° 18′)

V. Results and Discussion

A. Regular waves

The results for the q-factor for the PA, flap and Mixed farms in regular waves between 3 and 12 s are shown in Fig. 11, Fig. 12 and Fig. 13 respectively. Wave height of 1 m is considered for all periods. For these plots, a discretization of 0.25 s was utilized for the wave period T. When considering regular wave conditions and the considered metrics, the wave height is irrelevant since the power is proportional to the square of the wave height, which remains the same for each regular wave frequency. Since all the considered metrics, consider the ratios of power, this term is cancelled out.

Considering the PA mono-farms, the best q-factor is obtained for the WECA-PA-STAG-0 and WECA-PA-STAG-180 of 2.12 at 3.75 s. Both these are symmetric with respect to the wave directions, hence giving the same value. In general, most PA mono-array show constructive effects between 3 and 5.5 s.

Considering the flap mono-farms, the best q-factor is obtained for the WECA-FL-STAG-0 and WECA-PA-STAG-180 of 1.77 at 4.75 s. Both these are symmetric with respect to these wave directions, hence giving the same value. The FL mono-array in staggered and rectangular configuration show constructive effects between 3 to 8 s. For both PA and FL, the most constructive mono-farms are observed with the staggered configuration, owing to the lack of shadowing from the first row of WECs on the second and vica-versa.

Considering the Mixed farms, the best q-factor of 5.7 is achieved by WECA-MIX-RECT-0 at 4.75 s, which is much higher than the mono-farms. This high constructive effect is however localized close to 3.75 s. High q-factors greater than 2.12 are observed for multiple mixed array cases, with constructive effects shown between 3 and 10 s with the staggered configuration (WECA-MIX-STAG-0 and WECA-MIX-STAG-180) performing best across the most periods. It is very

likely, that resonances and the resulting reflections occurring at these periods are resulting in these high q-factors, thus drastically improving the performance of the mixed array. Furthermore, the PTO coefficient is obtained without any force or displacement constraints, which allow for such high values.

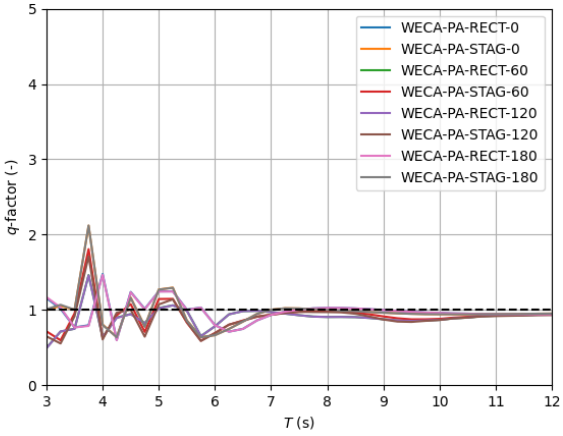

Fig. 11. q-factor for PA mono-farms in regular waves

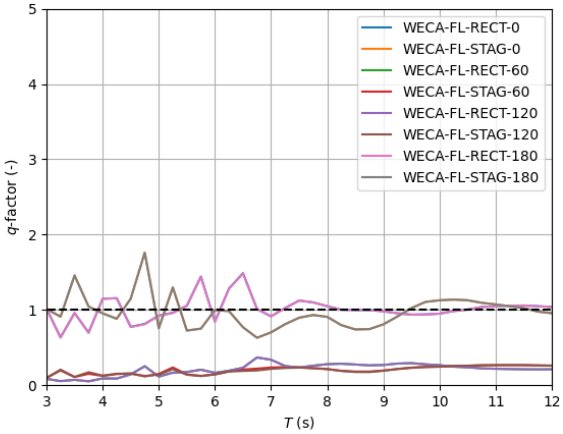

Fig. 12. q-factor for flap mono-farms in regular waves

Fig. 14 shows the H-factor for the mixed farms across different wave periods. This factor directly compares if the mixed farm is more constructive (H >1) or destructive (H <1) with respect to the mono-farms considering farm effects for both. It can be observed that multiple mixed farm cases perform better than the corresponding mono-farm cases in the considered periods from 3 to 12 s. For some periods (4.75 s and 6.75 s), the performance is up to 6.7 times better. It should be noted that while the mono-farms are destructive during some wave periods between 3 to 12 s, having a H >1 indicates that the mixed array configurations is less destructive, thus also performing better than mono-array during these periods.

Fig. 15 shows the M-factor for the mixed farms across different wave periods. This factor normalizes the differences in the power produced from the devices due to differences in their dimensions, thus including

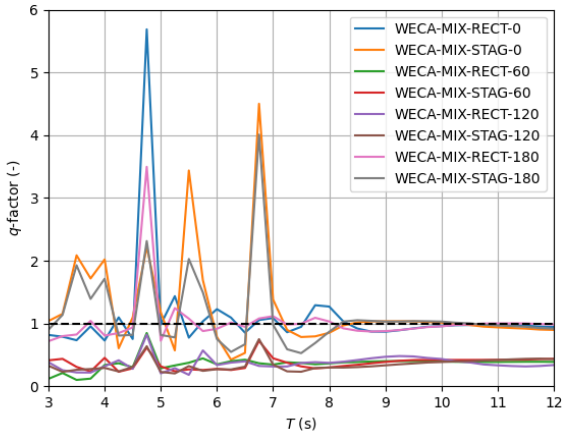

Fig. 13. q-factor for PA and flap mixed farms in regular waves

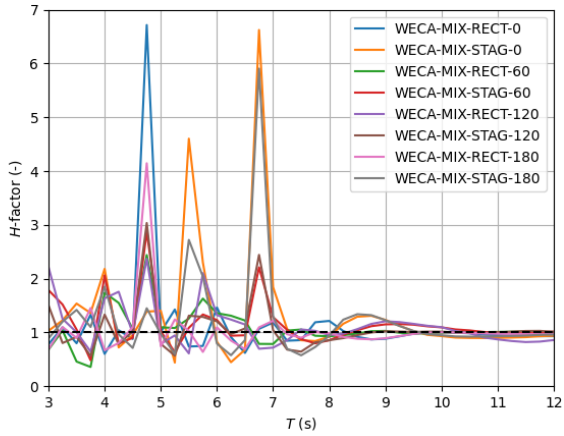

Fig. 14. H-factor for PA and flap mixed farms in regular waves

the effect of the hydrodynamic interaction between the devices as well as the dimensions of the devices themselves. M >1 indicates the mixed array having a higher capture width ratio than when considering both the mono-farms. It can be observed that the trend with M-factor is similar to the H-factor, with different mixed farms performing better than the mono-farms in the considered periods from 3 to 12 s. For some periods (4.75 s and 6.75 s), the performance is up to 7.5 times better. The higher M-factor values as compared to H-factor, also indicates that when considering the power/characteristic dimension (D for PA and W for flap) of the WEC, the hydrodynamic efficiency of mixed array is actually higher than when just considering the power.

B. *Irregular waves*

The results considering irregular waves is shown to obtain an estimation of the behavior of mixed and mono-farms considering realistic sea states.

The results for the q-factor for the PA, flap and Mixed farms in irregular waves with peak periods between 3 and 12 s and H_s=1 m are shown in Fig. 16, Fig. 17 and Fig. 18 respectively. For these plots, a discretization of 0.5 s was utilized for the peak period T_p.

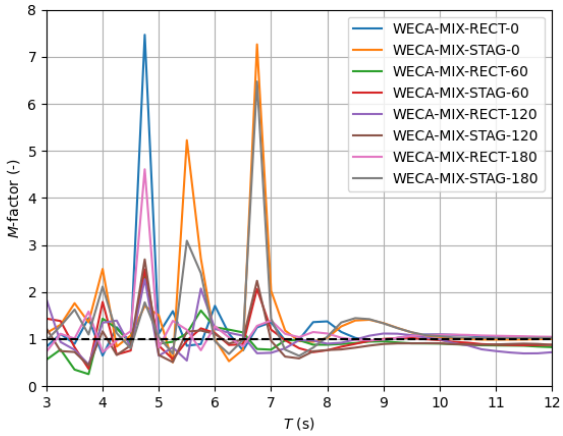

Fig. 15. M-factor for PA and flap mixed farms in regular waves

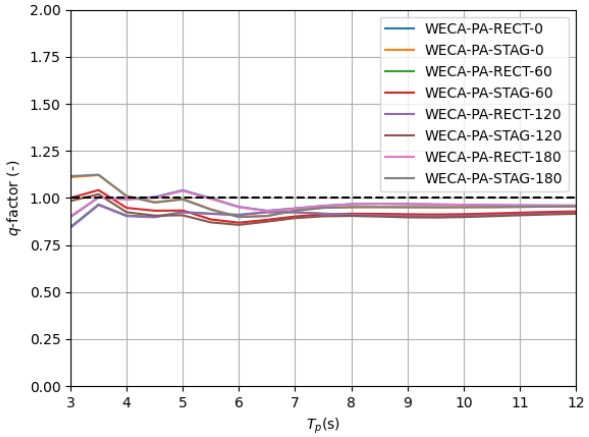

Fig. 16. q-factor for PA mono-farms in irregular waves (H_s = 1 m)

Considering the PA mono-farms, the best q-factor is obtained for the WECA-PA-STAG-0 and WECA-PA-STAG-180 of 1.12 at 3.75 s. Both these are symmetric with respect to the wave directions, hence giving the same value. PA mono-array cases WECA-PA-STAG-0/180 show constructive effects between 3 and 5 s, whiel WECA-PA-RECT-0/180 show constructive effects between 4.5 and 5.5 s. All the other cases are destructive.

Considering the flap mono-farms, the best q-factor is obtained for the WECA-FL-STAG-0 and WECA-PA-STAG-180 of 1.14 at 4 s. Both these are symmetric with respect to the wave directions, hence giving the same value. The FL mono-array cases WECA-FL-STAG-0/180 are constructive between 3 and 5 s, while WECA-FL-RECT-0/180 are constructive between 5.75 and 8.25 s.

For both PA and FL, similar to when considering regular waves, the most constructive mono-farms are observed with the staggered configuration, owing to the lack of shadowing from the first row of WECs on the second and vica-versa.

Considering the Mixed farms, the best q-factor of 1.17 is achieved by WECA-MIX-STAG-0 at 7 s, which is slightly higher than the mono-farms. It is however interesting to observe that multiple mixed array cases (WECA-MIX-STAG-0/180, WECA-MIX-RECT-0) are constructive across a wider range of periods from 3 to 9 s.

Fig. 19 shows the H-factor for the mixed farms across different wave periods considering irregular waves. It can be observed that almost all mixed array cases perform better than the mono-farms either by being more constructive or less destructive in the considered range of periods. For some periods (6 s and 7 s), the performance is up to 1.4 to 2.2 times better.

Fig. 20 shows the M-factor for the mixed farms across different wave periods considering irregular waves. It can be observed that the trend with M-factor is similar to the H-factor, with most mixed array cases performing better than the mono-farms in the considered periods from 3 to 12 s. For some periods (6 s and 7 s), the performance is 1.6 to 2.1 times better.

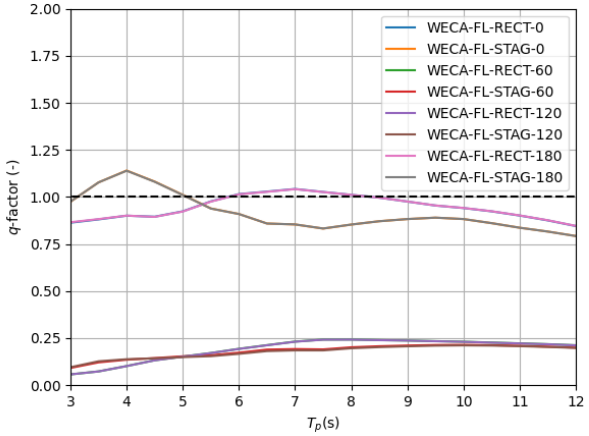

Fig. 17. q-factor for flap mono-farms in irregular waves (H_s = 1 m)

VI. Conclusion

This work, for the very first time, showcases the hydrodynamics and power produced by wave farms comprising of devices with different geometries, operating in different degrees of freedom, referred to as mixed farms. The WECs considered include PAs and flaps, considering both regular and irregular waves. When considering the irregular waves, sea states with significant wave height H_s = 1 m were considered, based on a location off the Dutch coast, where most range of peak period T_p was observed for the same H_s. Optimized PTO damping considering viscous losses (based on spectral domain method), and interactions between devices, resulting in a weakly non-linear frequency domain model is used to model both devices.

For the farms, 10 devices were considered. Two configurations (staggered and rectangular) and four incident wave angles (0, 60, 120 and 180) resulted in a total of 24 farm cases considering both mono and mixed farms.

In order to compare mono and mixed farms, three different metrics are used - q-factor, H-factor, and the newly introduced M factor. q-factor is well known, focusing on whether the wave farm is constructive or de-

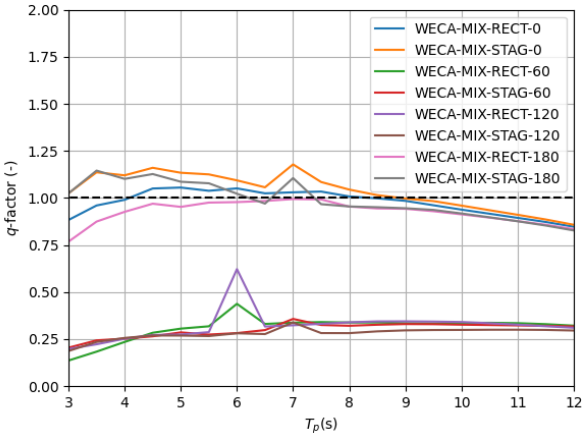

Fig. 18. q-factor for PA and flap mixed farms in irregular waves (H_s = 1 m)

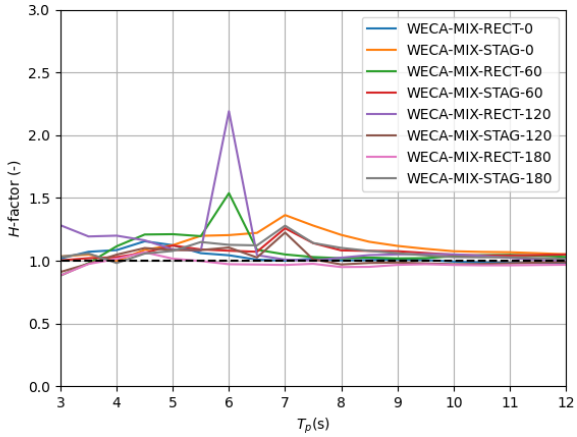

Fig. 19. H-factor for PA and flap mixed farms in irregular waves (H_s = 1 m)

structive with respect to the devices in isolation, when considering the power absorbed. H-factor, focuses on whether the mixed farm is constructive or destructive with respect to the mono farms, when considering the power absorbed. The newly introduced M-factor focuses on the capture width ratio of the mixed farms as compared to the mono farms, thus considering both the total power produced as well as the characteristic dimensions of the individual WECs in the farm. This is especially relevant, since the two different types of WECs have very different dimensions.

Mixed farms consistently outperform mono-farms across a wide range of wave periods, particularly when arranged in a staggered configuration. Under regular wave conditions, the q-factor for mixed arrays reaches up to 5.7, significantly higher than the maximum of 2.12 observed for mono-farms. Correspondingly, the H and M factors show improvements of up to 6.7 and 7.5 times, respectively, compared to mono-farms. Under irregular wave conditions, mixed arrays achieve a maximum q-factor of 1.17 and demonstrate constructive behavior over a broader range of peak periods than mono-farms, which tend to be destructive in several

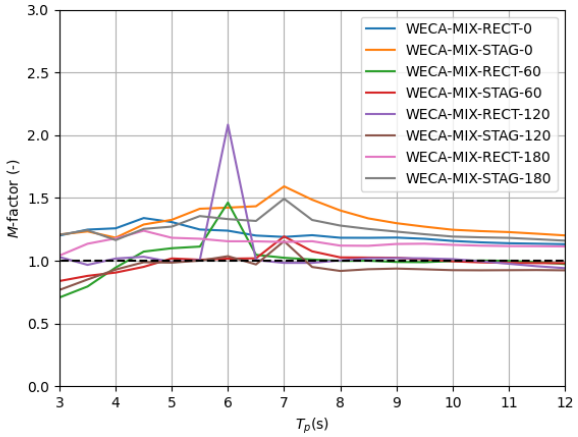

Fig. 20. M-factor for PA and flap mixed farms in irregular waves (H_s = 1 m)

cases. The M-factor consistently exceeds the H-factor, indicating that the hydrodynamic efficiency of mixed farms—when accounting for the differences in device dimensions—is superior to that of mono-farms. These findings highlight the potential of mixed wave energy converter arrays to improve overall power capture and system robustness in realistic sea states.

With this study, it can be observed that mixed farms show significant promise. By providing consistently higher power, across a range of sea states with higher hydrodynamic efficiency as compared to mono farms, they will potentially contribute towards the accelerated development of wave energy, thus bringing energy transition even closer.

ACKNOWLEDGEMENT

The authors would also like to acknowledge SURF and access to the HPC Snellius for running the simulations in HAMS-MREL, under project EINF3290.

REFERENCES

[1] (2024) North sea. [Online]. Available: https://energy.ec.europa.eu/topics/renewable-energy/offshore-renewable-energy_en
[2] (2024) Corpower. [Online]. Available: https://corpowerocean.com/corpack/
[3] (2024) Aw waveroller. [Online]. Available: https://aw-energy.com/utility-scale-power/
[4] (2025) Hiwave-5 project. [Online]. Available: https://www.hiwave-5.eu/about-us/
[5] (2024) Ondep project. [Online]. Available: https://www.ondep-wave.eu/
[6] J. Falnes and P. McIver, "Surface wave interactions with systems of oscillating bodies and pressure distributions," *Applied Ocean Research*, vol. 7, no. 4, pp. 225–234, 1985. [Online]. Available: https://www.sciencedirect.com/science/article/pii/014111878590029X
[7] S. Mavrakos, "Hydrodynamic coefficients for groups of interacting vertical axisymmetric bodies," *Ocean Engineering*, vol. 18, no. 5, pp. 485–515, 1991. [Online]. Available: https://www.sciencedirect.com/science/article/pii/002980189190027N
[8] J. Falnes and J. Todalshaug, "Heaving buoys, point absorbers and arrays," *Philosophical transactions. Series A, Mathematical, physical, and engineering sciences*, vol. 370, pp. 246–77, 01 2012.
[9] H. Wolgamot, P. Taylor, and R. Eatock Taylor, "The interaction factor and directionality in wave energy arrays," *Ocean Engineering*, vol. 47, pp. 65–73, 2012. [Online]. Available: https://www.sciencedirect.com/science/article/pii/S0029801812001138

[10] J. C. McNatt, V. Venugopal, and D. Forehand, "A novel method for deriving the diffraction transfer matrix and its application to multi-body interactions in water waves," *Ocean Engineering*, vol. 94, pp. 173–185, 2015. [Online]. Available: https://www.sciencedirect.com/science/article/pii/S0029801814004417

[11] G. Tokić and D. K. Yue, "Hydrodynamics of large wave energy converter arrays with random configuration variations," *Journal of Fluid Mechanics*, vol. 923, p. R1, 2021.

[12] T. Vervaet, V. Stratigaki, F. Ferri, L. De Beule, H. Claerbout, B. De Witte, M. Vantorre, and P. Troch, "Experimental modelling of an isolated wecfarm real-time controllable heaving point absorber wave energy converter," *Journal of Marine Science and Engineering*, vol. 10, no. 10, 2022. [Online]. Available: https://www.mdpi.com/2077-1312/10/10/1480

[13] S.-H. Yang, J. W. Ringsberg, and E. Johnson, "Wave energy converters in array configurations—influence of interaction effects on the power performance and fatigue of mooring lines," *Ocean Engineering*, vol. 211, p. 107294, 2020. [Online]. Available: https://www.sciencedirect.com/science/article/pii/S0029801820303371

[14] B. Borgarino, A. Babarit, and P. Ferrant, "Impact of wave interactions effects on energy absorption in large arrays of wave energy converters," *Ocean Engineering*, vol. 41, pp. 79–88, 2012. [Online]. Available: https://www.sciencedirect.com/science/article/pii/S0029801812000054

[15] M. Penalba, I. Touzón, J. Lopez-Mendia, and V. Nava, "A numerical study on the hydrodynamic impact of device slenderness and array size in wave energy farms in realistic wave climates," *Ocean Engineering*, vol. 142, pp. 224–232, 2017. [Online]. Available: https://www.sciencedirect.com/science/article/pii/S0029801817303517

[16] R. J. Bergillos, C. Rodriguez-Delgado, J. Allen, and G. Iglesias, "Wave energy converter configuration in dual wave farms," *Ocean Engineering*, vol. 178, pp. 204–214, 2019. [Online]. Available: https://www.sciencedirect.com/science/article/pii/S0029801819300939

[17] *Wave Energy Farm Assessment in Real Wave Climates: The North Sea*, ser. International Conference on Offshore Mechanics and Arctic Engineering, vol. Volume 7: Ocean Renewable Energy, 06 2024. [Online]. Available: https://doi.org/10.1115/OMAE2024-120946

[18] S. Bozzi, M. Giassi, A. Moreno Miquel, A. Antonini, F. Bizzozero, G. Gruosso, R. Archetti, and G. Passoni, "Wave energy farm design in real wave climates: the italian offshore," *Energy*, vol. 122, pp. 378–389, 2017. [Online]. Available: https://www.sciencedirect.com/science/article/pii/S0360544217301019

[19] B. Child and V. Venugopal, "Optimal configurations of wave energy device arrays," *Ocean Engineering*, vol. 37, no. 16, pp. 1402–1417, 2010. [Online]. Available: https://www.sciencedirect.com/science/article/pii/S0029801810001447

[20] Y. Peña-Sanchez, D. García-Violini, M. Penalba, A. Zarketa-Astigarraga, F. Ferri, V. Nava, and J. V. Ringwood, "Control co-design for wave energy farms: Optimisation of array layout and mooring configuration in a realistic wave climate," *Renewable Energy*, vol. 227, p. 120506, 2024. [Online]. Available: https://www.sciencedirect.com/science/article/pii/S0960148124005718

[21] M. Giassi and M. Göteman, "Layout design of wave energy parks by a genetic algorithm," *Ocean Engineering*, vol. 154, pp. 252–261, 2018. [Online]. Available: https://www.sciencedirect.com/science/article/pii/S0029801818301045

[22] M. Göteman, J. Engström, M. Eriksson, and J. Isberg, "Optimizing wave energy parks with over 1000 interacting point-absorbers using an approximate analytical method," *International Journal of Marine Energy*, vol. 10, pp. 113–126, 2015. [Online]. Available: https://www.sciencedirect.com/science/article/pii/S2214166915000119

[23] J. Engström, M. Eriksson, M. Göteman, J. Isberg, and M. Leijon, "Performance of large arrays of point absorbing direct-driven wave energy converters," *Journal of Applied Physics*, vol. 114, no. 20, p. 204502, 11 2013. [Online]. Available: https://doi.org/10.1063/1.4833241

[24] N. Faedo, Y. Peña-Sanchez, E. Pasta, G. Papini, F. D. Mosquera, and F. Ferri, "Swell: An open-access experimental dataset for arrays of wave energy conversion systems," *Renewable Energy*, vol. 212, pp. 699–716, 2023. [Online]. Available: https://www.sciencedirect.com/science/article/pii/S0960148123006924

[25] P. Balitsky, N. Quartier, G. Verao Fernandez, V. Stratigaki, and P. Troch, "Analyzing the near-field effects and the power production of an array of heaving cylindrical wecs and oswecs using a coupled hydrodynamic-pto model," *Energies*, vol. 11, no. 12, 2018. [Online]. Available: https://www.mdpi.com/1996-1073/11/12/3489

[26] Z. Y. Tay and V. Venugopal, "Hydrodynamic interactions of oscillating wave surge converters in an array under random sea state," *Ocean Engineering*, vol. 145, pp. 382–394, 2017. [Online]. Available: https://www.sciencedirect.com/science/article/pii/S0029801817305310

[27] J. C. McNatt, A. Porter, and K. Ruehl, "Comparison of numerical methods for modeling the wave field effects generated by individual wave energy converters and multiple converter wave farms," *Journal of Marine Science and Engineering*, vol. 8, no. 3, 2020. [Online]. Available: https://www.mdpi.com/2077-1312/8/3/168

[28] S. Zheng, Y. Zhang, and G. Iglesias, "Power capture performance of hybrid wave farms combining different wave energy conversion technologies: The h-factor," *Energy*, vol. 204, p. 117920, 2020. [Online]. Available: https://www.sciencedirect.com/science/article/pii/S0360544220310276

[29] M. Göteman, "Wave energy parks with point-absorbers of different dimensions," *Journal of Fluids and Structures*, vol. 74, pp. 142–157, 2017. [Online]. Available: https://www.sciencedirect.com/science/article/pii/S0889974617301627

[30] A. M. Ermakov, Z. A. Ali, K. Mahmoodi, O. Mason, and J. V. Ringwood, "Optimisation of heterogeneous wave energy converter arrays: A control co-design strategy," *Renewable Energy*, vol. 244, p. 122637, 2025. [Online]. Available: https://www.sciencedirect.com/science/article/pii/S096014812500299X

[31] H. Abdulkadir and O. Abdelkhalik, "Optimization of heterogeneous arrays of wave energy converters," *Ocean Engineering*, vol. 272, p. 113818, 2023. [Online]. Available: https://www.sciencedirect.com/science/article/pii/S0029801823002020

[32] M. F. Alday, V. Raghavan, and G. Lavidas, "Analysis of the north atlantic offshore energy flux from different reanalysis and hindcasts," in *Vol. 15 (2023): Proceedings of the European Wave and Tidal Energy Conference*, vol. 15. EWTEC, 2023.

[33] P. Laporte Weywada, "D1.1 advanced wave-structure interaction model – theory and user manual," *Zenodo*, 2018.

[34] J. Hals, T. Bjarte-Larsson, and J. Falnes, "Optimum Reactive Control and Control by Latching of a Wave-Absorbing Semisubmerged Heaving Sphere," ser. International Conference on Offshore Mechanics and Arctic Engineering, vol. 21st International Conference on Offshore Mechanics and Arctic Engineering, Volume 4, 06 2002, pp. 415–423. [Online]. Available: https://doi.org/10.1115/OMAE2002-28172

[35] L. S. P. da Silva, B. S. Cazzolato, N. Y. Sergiienko, B. Ding, H. M. Morishita, and C. P. Pesce, "Statistical linearization of the morison's equation applied to wave energy converters," *Journal of Ocean Engineering and Marine Energy*, vol. 6, no. 2, pp. 157–169, 2020. [Online]. Available: https://doi.org/10.1007/s40722-020-00165-9

[36] V. Raghavan, E. Loukogeorgaki, N. Mantadakis, A. V. Metrikine, and G. Lavidas, "HAMS-MREL, a new open source multiple body solver for marine renewable energies: Model description, application and validation," *Renewable Energy*, vol. 237, p. 121577, 2024. [Online]. Available: https://www.sciencedirect.com/science/article/pii/S0960148124016458

[37] V. Raghavan, A. Metrikine, G. Lavidas, T. Islam, and V. Venugopal, "Extension of hams with the generalized modes approach," in *Innovations in Renewable Energies Offshore - Proceedings of the 6th International Conference on Renewable Energies Offshore, RENEW 2024*, ser. Innovations in Renewable Energies Offshore - Proceedings of the 6th International Conference on Renewable Energies Offshore, RENEW 2024, C. Soares and S. Wang, Eds. CRC Press / Balkema - Taylor and Francis Group, 2024, pp. 193–199, 6th International Conference on Renewable Energies Offshore, RENEW 2024 ; Conference date: 19-11-2024 Through 21-11-2024.

[38] J. McNatt and C. Retzler, "The performance of the Mocean M100 wave energy converter described through numerical and physical modelling," *International Marine Energy Journal*, vol. 3, pp. 11–19, 05 2020.

[39] M. Folley and T. Whittaker, "Spectral modelling of wave energy converters," *Coastal Engineering*, vol. 57, no. 10, pp. 892–897, 2010. [Online]. Available: https://www.sciencedirect.com/science/article/pii/S0378383910000700

[40] L. Silva, N. Sergiienko, C. Pesce, B. Ding, B. Cazzolato, and H. Morishita, "Stochastic analysis of nonlinear wave energy converters via statistical linearization," *Applied Ocean Research*, vol. 95, p. 102023, 2020. [Online]. Available: https://www.sciencedirect.com/science/article/pii/S0141118719307230

[41] M. Folley and T. Whittaker, "Validating a spectral-domain model of an owc using physical model data," *International Journal of Marine Energy*, vol. 2, pp. 1–11, 2013. [Online]. Available: https://www.sciencedirect.com/science/article/pii/S2214166913000040

[42] M. F. Alday, V. Raghavan, and G. Lavidas, "Effects of wave spectrum representation on power production estimations from point absorbers," *SSRN*, 2025.

[43] J. Tan, W. Tao, A. J. Laguna, H. Polinder, Y. Xing, and S. Miedema, "A spectral-domain wave-to-wire model of wave energy converters," *Applied Ocean Research*, vol. 138, p. 103650, 2023. [Online]. Available: https://www.sciencedirect.com/science/article/pii/S0141118723001918

[44] O. M. Mazzaretto, M. Menéndez, and H. Lobeto, "A global evaluation of the jonswap spectra suitability on coastal areas," *Ocean Engineering*, vol. 266, p. 112756, 2022. [Online]. Available: https://www.sciencedirect.com/science/article/pii/S002980182202039X

[45] J. Falnes, "Radiation impedance matrix and optimum power absorption for interacting oscillators in surface waves," *Applied Ocean Research*, vol. 2, no. 2, pp. 75–80, 1980. [Online]. Available: https://www.sciencedirect.com/science/article/pii/0141118780900322

[46] T. Vervaet, N. Quartier, E. Carpintero Moreno, G. Verao Fernandez, F. Ferri, V. Stratigaki, and P. Troch, "System identification and centralised causal impedance matching control of a row of two heaving point absorber wave energy converters," *Ocean Engineering*, vol. 309, p. 118399, 2024. [Online]. Available: https://www.sciencedirect.com/science/article/pii/S0029801824017372

[47] M. Alday and G. Lavidas, "The echowave hindcast: A 30-years high resolution database for wave energy applications in north atlantic european waters," *Renewable Energy*, vol. 236, p. 121391, 2024. [Online]. Available: https://www.sciencedirect.com/science/article/pii/S0960148124014599